Polar Meteorol. Glaciol., **15**, 32–42, 2001

Behavior of externally mixed liquid and solid polar stratospheric cloud particles in a numerical box model under temperature decrease

Diana Daneva and Takashi Shibata

Solar Terrestrial Environment Laboratory, Nagoya University, Nagoya 464–8601

Abstract: Type I polar stratospheric clouds (PSCs) are simulated *via* an ensemble of externally mixed $H_2SO_4/HNO_3/H_2O$ ternary solution droplets and solid NAT (nitric acid tri-hydrate) particles in a microphysical box model. The behavior of this ensemble is investigated under two temperature-change conditions: meso- and synoptic-scale ones. The results show that the evolution of size and composition of liquid droplets depends strongly on temperature cooling rate, depletion of gas phase HNO_3, and initial size distribution; however, evolution of NAT particles is not strongly influenced by their initial size distribution. The development of the microphysical properties of the particles simulated in the model can be controlled by adjusting such parameters as cooling rate, total number of solid particles, and size distribution. The developed model can be used for interpreting lidar data of Arctic PSCs, and for simulating PSC particles. It can also be used in photochemical models investigating polar ozone depletion by providing the total surface area of the particles and the changes in gas phase HNO_3 due to condensation (evaporation) on these particles.

1. Introduction

Although polar stratospheric clouds (PSCs) have been observed in the Antarctic stratosphere for over a century (Stanford and Davis, 1974), they have been thought of as a relatively unimportant phenomenon in terms of atmospheric photochemistry. In 1986, however, one year after the first report of massive springtime ozone losses over Antarctica (Farman *et al.*, 1985), it was suggested that chemical reactions occurring on the surface of PSCs could play an important role in the observed ozone losses (*e.g.*, Solomon *et al.*, 1986). Since that time, many field, laboratory, and theoretical researches on heterogeneous atmospheric chemistry and microphysics of PSCs have been carried out. As a result, rapid progress has been made toward understanding the key role of the heterogeneous chlorine chemistry on PSCs in the formation of the Antarctic ozone hole. It is now believed that the ozone hole would not occur without the conversion of inactive chlorine reservoir forms, $ClONO_2$ and HCl, into reactive forms via heterogeneous reactions on PSCs (Ravishankara and Hanson, 1996). However, there are still many open questions concerning microphysics of PSCs and the mechanism of heterogeneous reactions (*e.g.,* Solomon, 1999).

PSCs are divided into two main types: type I and type II (*e.g.*, Poole *et al.*, 1988; Toon *et al.*, 1989). Type II PSCs are believed to form when the temperature drops

below the frost point of ice under given stratospheric conditions and to be composed of water ice (Steel *et al.*, 1983). Type I PSCs form at temperatures several degrees warmer than the ice frost point (Poole and McCormic, 1988). Although their exact composition and phase have not been established, type I PSCs are considered to be composed of liquid (type Ib) as well as of solid particles (type Ia). It is thought that liquid PSCs are probably composed of supercooled ternary solution droplets of HNO_3, H_2SO_4, and H_2O (Carslaw *et al.*, 1994; Drdla *et al.*, 1994). As for the solid particles, the main source of uncertainty in their chemical composition comes from the lack of understanding of their formation mechanism (Tolbert, 1994). Candidates for type Ia particles are NAT (nitric acid tri-hydrate) (*e.g.*, Crutzen and Arnold, 1986; Hanson and Mauersberger, 1988), NAD (nitric acid di-hydrate) (Worsnop *et al.*, 1993), NAT nucleated on SAT (sulfuric acid tetra-hydrate) (Iraci *et al.*, 1998), amorphous solid solutions of nitric and sulfuric acids (*e.g.*, Tabazadeh *et al.*, 1994), and so on.

Laboratory studies have shown that water ice, NAT, and liquid ternary solutions are all effective for activating chlorine heterogeneously (*e.g.*, Carslaw *et al.*, 1997a). While ice particles are highly reactive but not so abundant in Arctic as in the Antarctic due to their low formation temperature, NAT particles can exist at higher temperatures, but there are some uncertainties about their efficiency in ozone destroying reactions (Carslaw *et al.*, 1997b). In the case of liquid solutions, the activation of chlorine is comparable with that on NAT at the same temperature and even faster if at temperatures a few degrees above the ice frost point (Ravishankara and Hanson, 1996). Moreover, modeled ozone depletion is greater when liquid aerosols persist through the winter than when solid particles form (Carslaw *et al.*, 1997b). These facts underline the importance of liquid PSC (Type Ib) for ozone destruction processes.

A number of photochemical box models (*e.g.*, Müller *et al.*, 1994) have been developed to simulate observed ozone losses in both the Arctic and Antarctic regions. To estimate the impact of heterogeneous chemistry on ozone destruction these models make use of the total aerosol surface area available for heterogeneous reactions, information about a particle's phase, composition, formation mechanism, specific chemical reactivity of the surfaces and abundances of atmospheric gases involved in ozone destroying cycles.

In this paper, we present an attempt to simulate Type I PSCs through numerical modeling of an ensemble of liquid $H_2SO_4/HNO_3/H_2O$ ternary solution droplets externally mixed with NAT particles. Our model calculates the change of size and composition of liquid droplets and size of solid particles when undergoing synoptic or meso-scale temperature fluctuations under winter polar stratospheric conditions, and it also calculates the resulting depletion of gas-phase HNO_3 and H_2O.

Such a model can provide the photochemical models, mentioned above, with data for total aerosol surface area, particle composition, and depletion of gas phase. Also through parameterization of the model, interpretation of lidar data of PSCs can be made (Shibata, 1999) in attempt to achieve better understanding of the formation mechanism and composition of these clouds.

2. Numerical model

The model assumes that the PSC particles are an ensemble of externally mixed liquid ternary solution droplets of H_2SO_4, HNO_3, and H_2O and solid NAT particles. The evolution of the particles is calculated under adiabatic cooling and warming within meso- and synoptic-scale temperature fluctuations. Particles interact only with gas phase molecules through evaporation and condensation of H_2O and HNO_3. And no formation of new particles, coagulation or sedimentation of particles occurs. The variation of concentration of gas-phase molecules as a result of condensation and evaporation is simultaneously calculated. The concentration of H_2SO_4 in the particles and in the atmosphere is assumed not to change because of its very low ambient atmospheric pressure and involatility at the assumed temperatures.

The condensation and evaporation equations (Pruppacher and Klett, 1997; Hamill *et al.*, 1977) are of the form

$$\frac{dn_i}{dt} = \frac{4\pi r D_i (P_i - K_i Pvap_i)}{(1+\lambda_i Kn_i) kT}, \tag{1}$$

where the suffix $i=1$ or 2 corresponds to H_2O and HNO_3 respectively, n_i is the number of molecules of i-th species in the particle, P_i is the partial pressure of the i-th gas, Kn_i is the Knudsen number, r is the particle radius, k is the Boltzmann constant, and T is temperature. $Pvap_i$ denotes the vapor pressure of the i-th gas over a flat surface. For liquid particles, $Pvap_i$ is calculated according to Luo *et al.* (1995). NAT particles are assumed to have constant composition (HNO_3 : H_2O = 1 : 3) and be in equilibrium with water vapor in the environment. Their vapor pressure depends only on temperature and water vapor partial pressure (Hanson and Mauersberger, 1988).

The diffusion coefficient D_i and correction factor λ_i are (Fuchs and Sutugin, 1971)

$$D_i = \frac{l_i}{3}\sqrt{\frac{8kT}{\pi m_i}}, \tag{2}$$

and

$$\lambda_i = \frac{1.333 + 0.71 Kn_i^{-1}}{1 + Kn_i^{-1}} + \frac{4(1-\alpha)}{3\alpha}. \tag{3}$$

Here m_i and l_i are the mass of a molecule of the i-th species in the particle and the mean free path for this molecule in air. The "sticking coefficient" α is assumed to be unity. We are interested in the growth of particles with initial radii between 0.01 and 1 μm while the mean free path in the considered stratospheric conditions is of order 1 μm. Therefore, we are treating growth or evaporation throughout the range from small to large Knudsen number. Equation (1) takes account of the smooth transition between diffusively controlled gas uptake (large particles with $Kn \ll 1$) and kinetically limited uptake in the Knudsen regime (small particles with $Kn \gg 1$).

The growth rate of the particles is given by (Pruppacher and Klett, 1997; Hamill *et al.*, 1977)

$$\frac{dr}{dt}=\sum_{i=1}^{2}\frac{dr}{dn_i}\frac{dn_i}{dt}=\sum_{i=1}^{2}\frac{V_i D_i (P_i-K_i Pvap_i)}{r(1+\lambda_i Kn_i)kT}, \tag{4}$$

since $dr/dn_i=V_i/4\pi r^2$. Here V_i is the partial molar volume of the i-th component in the ternary solution. The rest of the notations are the same as above.

The Kelvin term for ternary solution droplets is calculated from

$$K_i=\exp\left[\frac{2\sigma V_i}{R_A Tr}\right], \tag{5}$$

where σ is the liquid/gas surface energy, assumed to be 90 erg/cm^2 (Meilinger *et al.*, 1995), R_A is the universal gas constant and V_i is the partial molar volume of the i-th component in the ternary solution, estimated with the calculation program provided by Krieger *et al.* (2000). K_i takes account of the elevation of the vapor pressure over a curved droplet to that over an infinite flat surface. It must be noted that accurate calculation of the Kelvin term K_i for stratospheric droplets is difficult due to lack of reliable data for σ under stratospheric temperatures (Carslaw *et al.*, 1997a). For particle radii of interest (0.01–1 μm), the Kelvin term for the smallest droplets can reach values sufficient to suppress their growth if either the cooling is too slow or the temperature amplitude is not high enough (Meilinger *et al.*, 1995).

We did not take into account the Kelvin effect of NAT particles, because (1) there are no reliable data about solid/vapor surface energy of NAT and (2) the saturation ratio of NAT at assumed stratospheric gaseous composition, temperature range, and total number of solid particles, is high enough ($S\approx 2$) that taking into account the Kelvin term would not significantly affect the solid particles' growth. As well, NAT particles grow beyond the size, influenced by Kelvin effect ($r<0.1\,\mu$m) very soon after beginning of cooling because of their high supersaturation with respect to HNO_3.

Equation (1) is solved numerically by using a fourth order Runge-Kutta scheme. The radii of both liquid and solid particles are calculated from:

$$r=\left[\frac{3}{4\pi}\frac{m}{\rho}\right]^{1/3}, \tag{6}$$

where $m=\sum_i n_i m_i$ is the mass of a particle, m_i being the mass of a molecule of the i-th species and n_i the number of molecules of the i-th species in a particle. For ternary solution droplets, $i=1$, 2 or 3 corresponding to H_2O, HNO_3, or H_2SO_4, respectively. For solid NAT particles, $i=1$ or 2 because they are assumed to have fixed composition (HNO_3 : $H_2O=1$: 3). The density ρ of the ternary solution is estimated by the numerical code of Krieger *et al.* (2000) for corresponding weight percentages and temperatures. For NAT particles, $\rho=1.62$ g/cm^3 (Taesler *et al.*, 1975).

The growth of the particles is calculated by using the Lagrangian scheme in radial space. The initial size distribution of liquid droplets and that of NAT particles are set to be lognormal, with 0.075-μm mode radius and mode width of 1.86 and are shown in Figs. 4 and 5 with filled circles. The total particle concentration N_{tot} is 9.99 cm^{-3} for a ternary solution and 0.01 cm^{-3} for NAT. The size range is set initially from 0.01 to 1 μm and represented by 30 size bins for both NAT and liquid droplets, separately. Each size bin consists of particles with given uniform radius and number, corresponding to

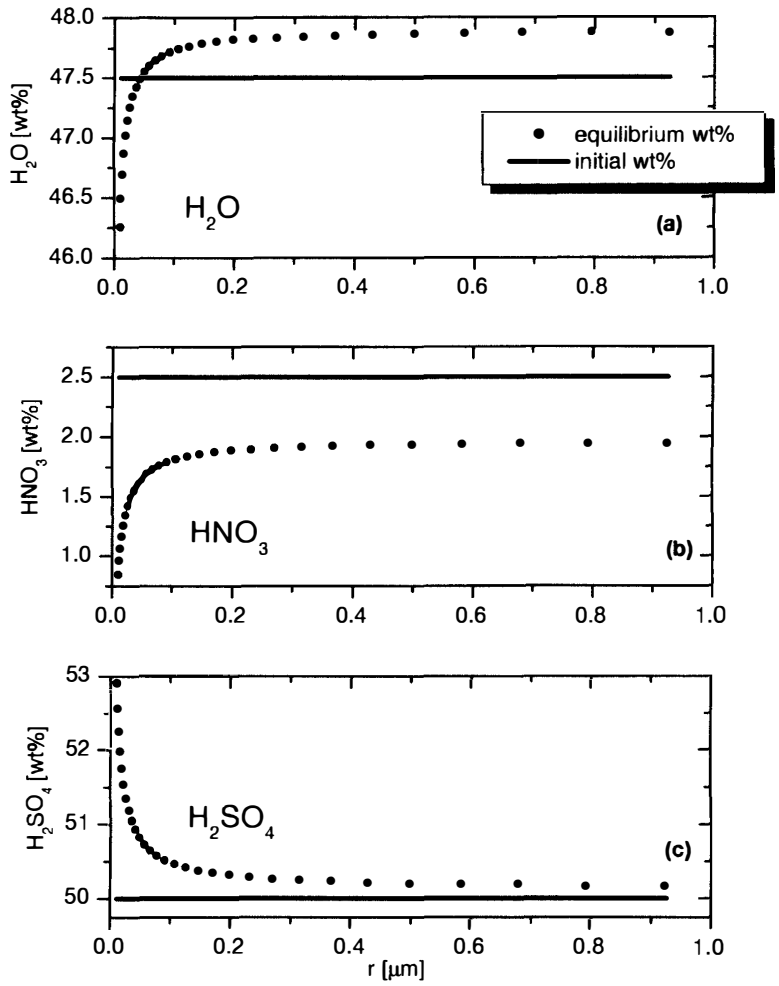

Fig. 1. Equilibrium composition of ternary solution droplets at T=196 K, total atmospheric pressure of 60 hPa, HNO_3 and H_2O mixing ratios of 5 ppmv and 10 ppbv, respectively. Thick solid lines represent the initial tentatively set composition of liquid ternary solution droplets. Dots represent the equilibrium composition for given conditions. Every dot corresponds to the size of the representative bin.

this radius from initial lognormal size distribution. The numbers of particles in each size bin do not change during simulations because of the use of the Lagrangian approach to the evolution of size bins. The initial concentrations of gas-phase H_2O and HNO_3 molecules are 5 ppmv and 10 ppbv, respectively. The total atmospheric pressure is 60 hPa at 196 K, and pressure is assumed to change with temperature via isentropic motion of air.

The initial composition of ternary droplets was tentatively set as 2.5 wt% HNO_3, 50 wt% H_2O, and 47.5 wt% H_2SO_4. They were allowed to reach equilibrium with the environment at constant temperature of 196 K before the beginning of cooling. The resulting compositions of the particles are used as the initial condition for the simulations. In this process of initial equilibration, NAT particles were not included in the model. As can be seen from Fig. 1, when in thermodynamic equilibrium with the gas phase, droplets tend to develop the same composition, irrespective of their size, unless

they are so small ($r<0.1\mu m$) that the Kelvin effect becomes important. Due to the Kelvin effect the amount of volatile species HNO_3 and H_2O in the smallest droplets is reduced, leading to higher H_2SO_4 concentration in these droplets.

3. Results and discussion

The evolution of an ensemble of the liquid ternary solution droplets externally mixed with solid NAT particles (described in Section 2) is investigated in the case of meso-scale temperature fluctuations and in the case of synoptic-scale ones.

In the first case, the cooling (and subsequent warming) rate is taken to be 6 K per hour, which corresponds to lee wave temperature perturbation, frequently observed before an appearance of PSCs in the Arctic. The temperature curve is shown in Fig. 2a. Evolution of the composition and size of the liquid particles is shown in Figs. 2c, 2d, and 2e for the particles in bins 1, 10, 16, 24 and 30. These bins are shown in Fig. 4 by

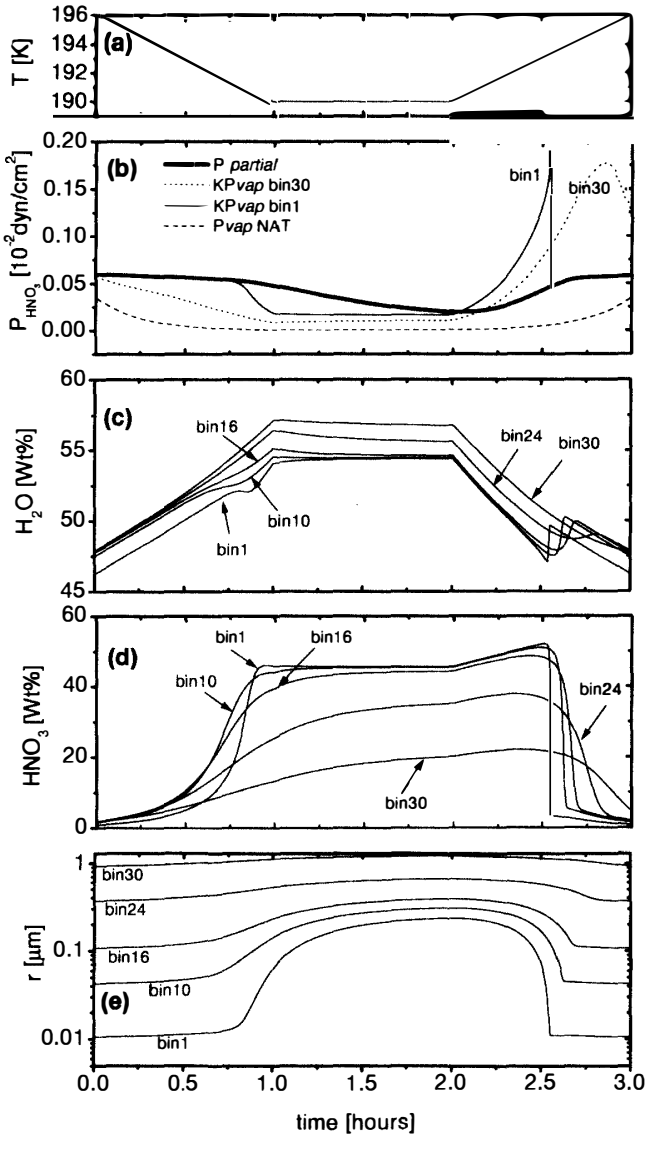

Fig. 2. Evolution of liquid particles size and composition within a lee wave cooling event with temperature change rate $\Delta T=6K$ per hour. (a) Changes of temperature with time. (b) HNO_3 partial pressure (thick solid line), HNO_3 vapor pressure of NAT (dashed line), vapor pressure of HNO_3 over curved surface for particles in bin 1 (thin solid line) and bin 30 (dotted line). (c) Evolution of weight percentage of H_2O in the droplets for bins 1, 10, 16, 24, and 30. (d) Evolution of weight percentage of HNO_3 in the droplets for bins 1, 10, 16, 24, and 30. (e) The evolution of radius of the droplets for the same size bins as above.

squares. Some size distributions after the cooling starts are also shown in the same figures. The development of the HNO_3 partial and vapor pressure for the smallest and largest size bins together with vapor pressure of NAT is given in Fig. 2b. The evolution of size distribution for ternary droplets and NAT particles is shown in Figs. 4a and 4b, respectively.

In this case of strong cooling, the temperature fluctuations force liquid particles to depart considerably from initial thermodynamic equilibrium, so their size and composition change significantly. The smallest droplets are able to overcome the Kelvin barrier because of the high cooling rate. They grow by more than a factor of 22 (bin 1 in Fig. 2e) and reach the composition of an almost binary HNO_3/H_2O solution (with only 0.005 wt% H_2SO_4) upon warming at about 193 K (Fig. 2d) (as reported also by Meilinger *et al.* (1995)). The largest droplets (bin 30 in Fig. 2e) grow only by a factor of 1.3 since their growth rate is proportional to $1/r$ (see eq. (4) for $Kn \ll 1$). When the warming starts two hours after the cooling begins, liquid particles begin to evaporate

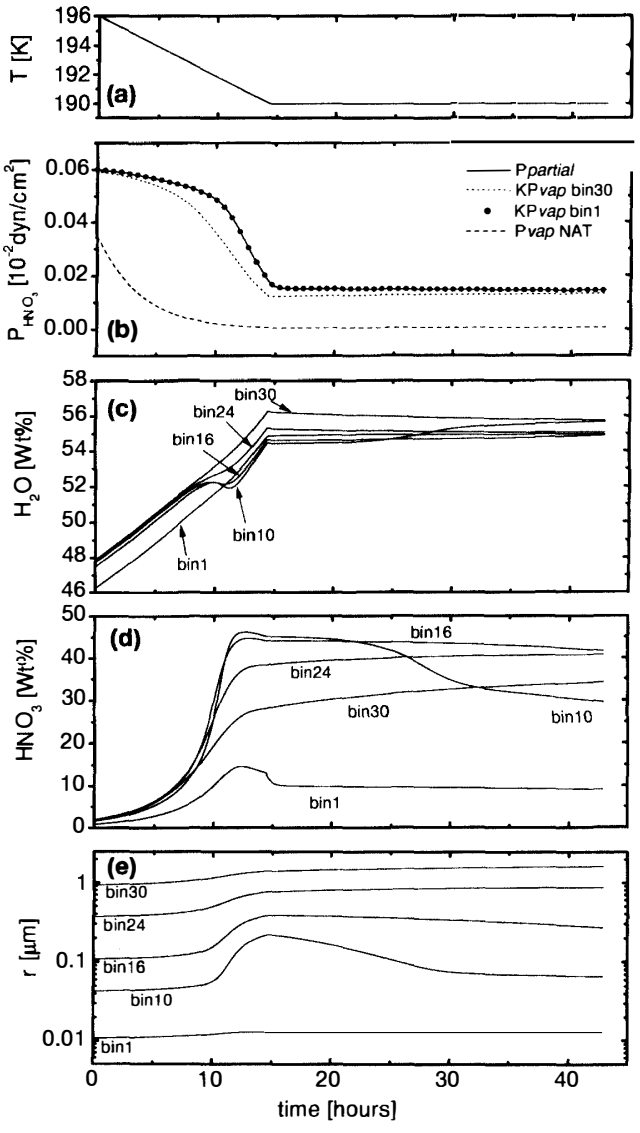

Fig. 3. Evolution of liquid particle size and composition within synoptic-scale cooling event with temperature change rate $\Delta T = 0.42$ K per hour. (a) Changes of temperature with time. (b) HNO_3 partial pressure (solid line), HNO_3 vapor pressure of NAT (dashed line), vapor pressure of HNO_3 over curved surface for particles in bin 1 (filled circles) and bin 30 (dotted line). (c) Evolution of weight percentage H_2O in the droplets for bins 1, 10, 16, 24, and 30. (d) Evolution of weight percentage of HNO_3 in the droplets for bins 1, 10, 16, 24, and 30. (e) Evolution of radius of the droplets for the same size bins as above.

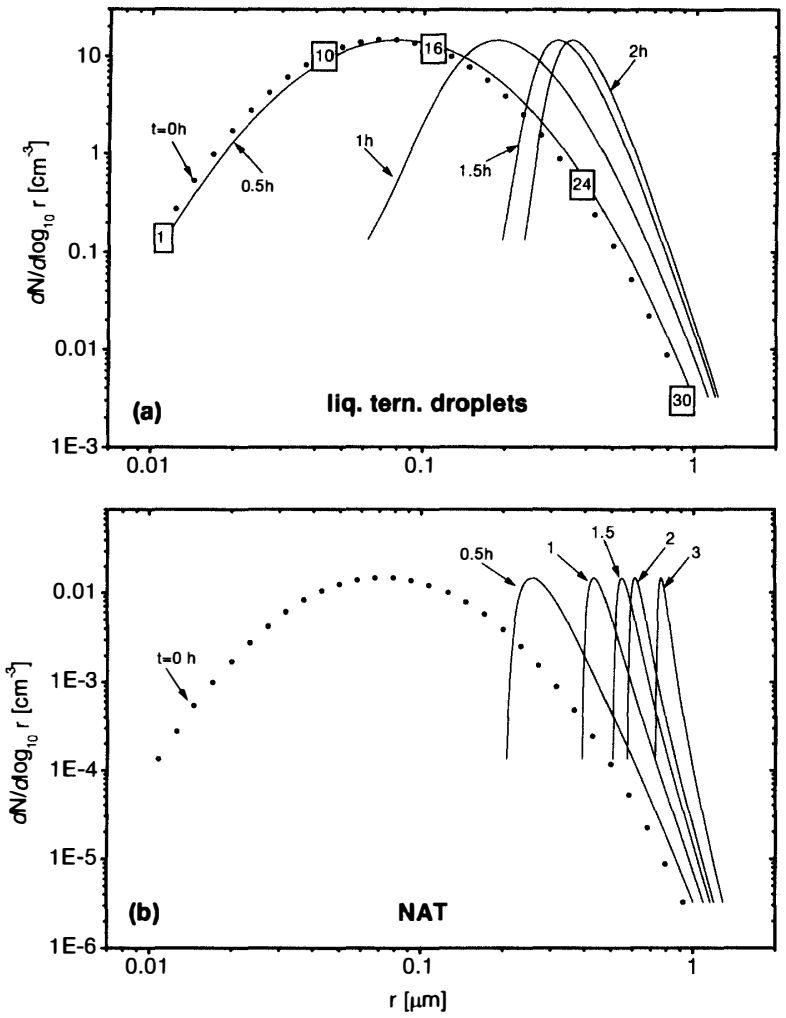

Fig. 4. Evolution of size distribution in strong lee wave cooling event with temperature change rate $\Delta T = 6\,K$ per hour. The size bins, whose evolution is followed in the presentation, are depicted by squares with the number of the bin inside. The time in hours after beginning of cooling (see Fig. 2a) is shown with numbers near the curves. The initial size distribution at $t = 0$ hours is depicted by small filled circles. (a) Evolution of size distribution for liquid droplets and (b) for NAT particles.

while solid particles continue to grow because they are still far from saturation in respect to HNO_3, *i.e.*, they have a saturation ratio $S > 1$ (Figs. 2b and 4). The highest HNO_3 concentration is in the smallest droplets during warming because evaporating HNO_3 leaves the particles more slowly than H_2O (Meilinger *et al.*, 1995).

The slower (synoptic scale) cooling rate is taken to be 10 K per day (or 0.42 K per hour), which is representative of PSC's synoptic-scale-temperature-histories in both Arctic and Antarctic regions. The evolution of the ensemble of NAT and ternary solution droplets is examined for two days.

For this case of slow cooling, the temperature curve and evolution of the size and composition of the liquid particles are shown in Figs. 3a, c, d and e. The change in size distribution is shown in Fig. 5 and the evolution of partial and vapor pressures of HNO_3 in Fig. 3b. Figure 3b shows that the smallest particles (bin 1, filled circles) always

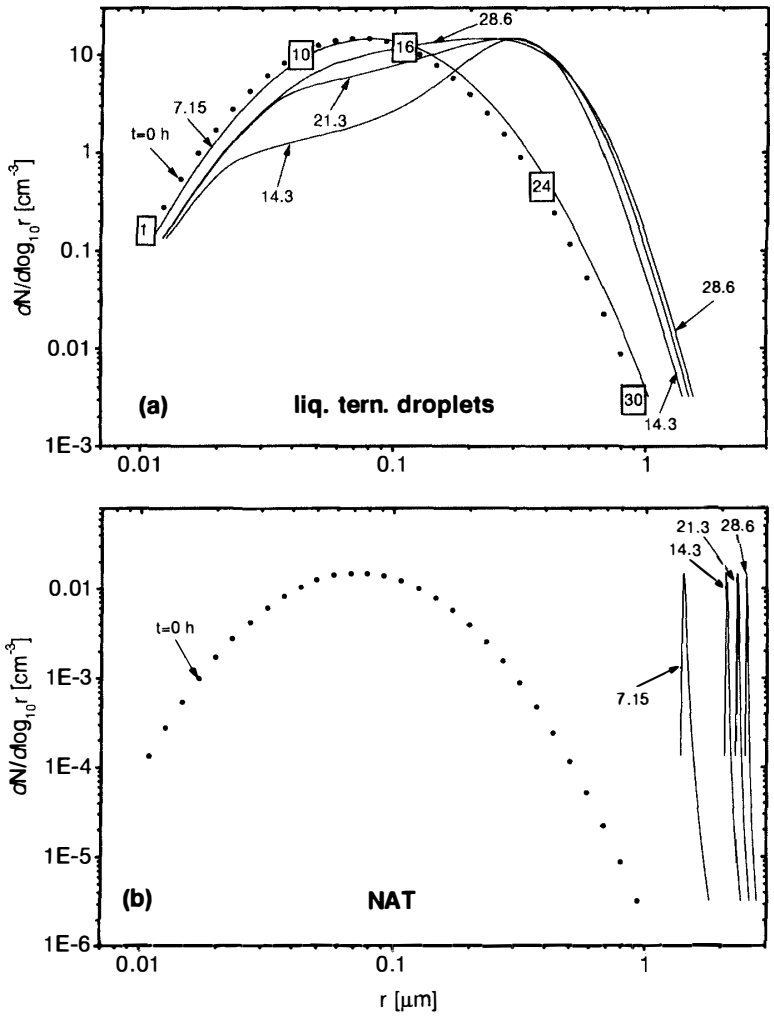

Fig. 5. Evolution of size distribution in slow synoptic cooling event with temperature change rate $\Delta T = 0.42\,K$ per hour. The size bins, whose evolution is followed in the presentation, are depicted by squares with the number of the bin inside. The time in hours after beginning of cooling (see Fig. 3a) is shown with numbers near the curves. The initial size distribution at $t = 0$ hours is depicted by small filled circles. (a) Evolution of size distribution for liquid droplets and (b) for NAT particles.

succeed in readjusting their vapor pressure to partial pressure changes (solid line), while the largest ones (bin 30, doted line) have a saturation ratio of $S > 1$. The continuous and slow cooling leads to substantial depletion of HNO_3 from the gas phase through condensation of HNO_3 on NAT and liquid particles. The depletion of gas phase H_2O through condensation is insignificant in our calculations because of its relatively large mixing ratio. Actually, most of the HNO_3 is depleted during the cooling in the first 14 hours, when NAT and medium-sized liquid particles grow very fast by uptake of nitric acid and water. The change in the sizes of the smallest droplets is small because of the Kelvin effect, which as mentioned in Section 2, can reduce the particle growth if the cooling is slow. The slow growth of large particles is due to diffusively hindered gas transfer to their surfaces as mentioned earlier in this section. As a result the medium-

sized droplets (bins 10 and 16 on Fig. 3d) reach the highest HNO_3 concentration now, in contrast with the strong cooling event case, in which the smallest ones did (bin 1).

After the cooling is terminated, the temperature is kept constant at 190 K for 30 hours. During this time, NAT particles and the largest droplets continue to grow and, thus, to deplete gas phase HNO_3 further. As a result, the smallest and the medium-sized droplets begin to evaporate in order to maintain in equilibrium with the constantly depleted environment. This process is clearly shown by the evolution of size distribution of liquid ternary solution droplets in Fig. 5a and of NAT particles in Fig. 5b. The same picture of evaporating medium- and small-sized droplets will appear even if an ensemble of only liquid ternary solution droplets is considered under the same conditions. This means that the total number of solid particles, $N_{tot}=0.01\ cm^{-3}$, used here does not significantly affect the evolution of liquid droplets by strongly depleting gas phase HNO_3 concentration. We took N_{tot} from Shibata (1999), who showed that N_{tot} from 0.001 to 0.01 cm^{-3} fits well his observations of PSCs. If a larger number of NAT particles is used (for example 1 cm^{-3}), the gas phase HNO_3 is depleted very quickly and particle growth is hindered. Also, the composition of liquid particles becomes nearly binary H_2O/H_2SO_4 with less than 1 wt% HNO_3.

4. Summary

We investigated the behavior of an ensemble of externally mixed liquid (H_2SO_4/HNO_3/H_2O ternary solution) and solid (NAT) particles under two temperature-change conditions: meso- and synoptic-scale ones. It was found that the evolution of the size and composition of liquid droplets depends strongly on temperature cooling rate, depletion of gas phase HNO_3, and initial size distribution; however, the evolution of NAT particles is not strongly influenced by their initial size distribution.

Our intention is to use the developed box model to simulate and interpret lidar data of Arctic PSCs. The model will also be used in photochemical models investigating polar ozone depletion by using data on total particle surface area.

References

Carslaw, K.S., Luo, B.P., Clegg, S.L., Peter, T., Brimblecombe, P. and Crutzen, P.J. (1994): Stratospheric aerosol growth and HNO_3 gas phase depletion from coupled HNO_3 and water uptake by liquid particles. Geophys. Res. Lett., **21**, 2479–2482.

Carslaw, K.S., Peter, T. and Clegg, L. (1997a): Modeling the composition of liquid stratospheric aerosols. Rev. Geophys., **35**, 125–154.

Carslaw, K.S., Peter, T. and Müller, R. (1997b): Uncertainties in reactive uptake coefficients for solid stratospheric particles, 2, Effect on ozone depletion. Geophys. Res. Lett., **24**, 1747–1750.

Crutzen, P.J. and Arnold, F. (1986): Nitric acid cloud formation in the cold Antarctic stratosphere: A major cause for the springtime ozone hole. Nature, **324**, 651–654.

Drdla, K., Tabazadeh, A., Turco, R.P., Jacobson, M.Z., Dye, J.E., Twohy, C. and Baumgardner, D. (1994): Analysis of the physical state of one Arctic polar stratospheric cloud based on observations. Geophys. Res. Lett., **21**, 2475–2478.

Farman, J.C., Gardiner, B.G. and Shanklin, J.D. (1985): Large losses of total ozone in Antarctica reveal seasonal ClO_x/NO_x interaction. Nature, **315**, 207–210.

Fuchs, N.A. and Sutugin, A.G. (1971): High dispersed aerosols. Topics in Current Aerosol Research, Vol. 2,

ed. by G.M. Hidy and J.R. Brock. Pergamon Press, 1–60.
Hamill, P., Toon, O.B. and Kiang, C.S. (1977): Microphysical processes affecting stratospheric aerosol particles. J. Atmos. Sci., **34**, 1104–1119.
Hanson, D.R. and Mauersberger, K. (1988): Laboratory studies of the nitric acid trihydrate: Implications for the south polar stratosphere. Geophys. Res. Lett., **15**, 855–858.
Iraci, L.T., Fortin, T.J. and Tolbert, M.A. (1998): Dissolution of sulfuric acid tetrahydrate at low temperatures and subsequent growth of nitric acid trihydrate. J. Geophys. Res., **103**, 8491–8498.
Krieger, U.K., Mössinger, J.C., Luo, B., Weers, U. and Peter, T. (2000): Measurement of the refractive indices of H_2SO_4-HNO_3-H_2O solutions to stratospheric temperatures. Appl. Opt., **39**, 3691–3703.
Luo, B.P., Carslaw, K.S., Peter, T. and Clegg, S. (1995): Vapor pressure of $H_2SO_4/HNO_3/H_2O$ solutions to low stratospheric temperatures. Geophys. Res. Lett., **22**, 247–250.
Meilinger, S.K., Koop, T., Luo, B., Huthwelker, T., Carslaw, K.S., Krieger, U., Crutzen, P.J. and Peter, T. (1995): Size-dependent stratospheric droplet composition in lee wave temperature fluctuations and their potential role in PSC freezing. Geophys. Res. Lett., **22**, 3031–3034.
Müller, R., Peter, Th., Crutzen, P., Oelhaf, H., Adrian, G., Clarmann, Th. v., Wegner, A., Schmidt, U. and Lary, D. (1994): Chlorine chemistry and the potential for ozone depletion in the arctic stratosphere in the winter of 1991/92. Geophys. Res. Lett., **21**, 1427–1430.
Pruppacher, H.R. and Klett, J.D. (1997): Microphysics of Clouds and Precipitation. Dordrecht, Kluwer Acad. Publ.
Poole, L.R. and McCormick, M.P. (1988): Polar stratospheric clouds and the ozone hole. J. Geophys. Res., **93**, 8423–8430.
Poole, L.R., Osborn, M.T. and Hunt, W.H. (1988): Lidar observations of arctic polar stratospheric clouds, 1988: signature of small, solid particles above the frost point. Geophys. Res. Lett., **15**, 867–870.
Ravishankara, A.R. and Hanson, D.R. (1996): Differences in the reactivity of type I PSC's depending on their phase. J. Geophys. Res.,**101**, 3885–3890.
Shibata, T. (1999): On the lidar-observed sandwich structure of polar stratospheric clouds (PSCs), 2, Numerical simulations of externally mixed PSC particles. J. Geophys. Res., **104**, 21613–21619.
Solomon, S. (1999): Stratospheric ozone depletion: a review of concepts and history. Rev. Geophys., **37**, 275–316.
Solomon, S., Garcia, R.R., Rowland, F.S. and Wuebbles, D.J. (1986): On the depletion of Antarctic ozone. Nature, **321**, 755–758.
Stanford, J.L. and Davis, J.S. (1974): A century of stratospheric cloud reports: 1870–1972. Bull. Am. Meteorol. Soc., **55**, 213–219.
Steel, H.M., Hamill, P., McCormick, M.P. and Swissler, T.J. (1983): The formation of polar stratospheric clouds. J. Atmos. Sci., **12**, 517–528.
Tabazadeh, A., Turco, R.P., Drdla, K., Jacobson, M.Z. and Toon, O.B. (1994): A study of type I polar stratospheric cloud formation. Geophys. Res. Lett., **21**, 1619–1622.
Taesler, I., Delaplane, R.G. and Olovsson, I. (1975): Hydrogen bond studies. XCIV. Diaquaoxonium ion in nitric acid trihydrate. Acta Cryst., **B31**, 1489–1492.
Tolbert, M.A. (1994): Sulfate aerosols and polar stratospheric cloud formation. Science, **264**, 527–528.
Toon, O.B., Turco, R.P., Jordan, J., Goodman, J. and Ferry, G. (1989): Physical processes in polar stratospheric ice clouds. J. Geophys. Res., **94**, 11359–11380.
Worsnop, D.R., Fox, L.E., Zahniser, M.S. and Wofsy, S.C. (1993): Vapor pressure of solid hydrates of nitric acid: Implications for polar stratospheric clouds. Science, **259**, 71–74.

(Received January 29, 2001; Revised manuscript accepted June 26, 2001)